Far East Journal of Mathematical Sciences (FJMS)

Published Online: July 2016
http://dx.doi.org/10.17654/MS100020315
Volume 100, Number 2, 2016, Pages 315-332 **ISSN: 0972-0871**

LATTICE BOLTZMANN SIMULATION OF FORCED CONVECTION IN NON-NEWTONIAN FLUID THROUGH LOW PERMEABLE POROUS MEDIA

M. Y. Gokhale and Ignatius Fernandes

Department of Mathematics
Maharashtra Institute of Technology
Pune, India
e-mail: mukundyg@yahoo.com

Department of Mathematics
Rosary College
Navelim, Goa, India
e-mail: ignatius4u@gmail.com

Abstract

Numerical simulation is carried out to study forced convection in non-Newtonian fluids flowing through low permeable porous media like sandstones and sand. Simulation is carried out using lattice Boltzmann method for both shear-thinning and shear-thickening, by varying the power-law index from 0.5 to 1.5 in Carreau-Yasuda model. Parameters involved in lattice Boltzmann method and Carreau model are identified to achieve numerical convergence. Permeability and porosity are varied in the range of 10^{-10} to 10^{-6} and 0.1 to 0.7, respectively, to match actual geometrical properties of sandstone. Numerical technology is validated by establishing Darcy's law

Received: January 21, 2016; Accepted: April 29, 2016
2010 Mathematics Subject Classification: 76S05.
Keywords and phrases: lattice Boltzmann method, Carreau-Yasuda model, non-Newtonian fluid, porous media.
Communicated by K. K. Azad

by plotting the graph between velocity and pressure gradient. Consequently, investigation is carried out to study the influence of material properties of porous media on flow properties such as velocity profiles, temperature profiles and Nusselt number.

1. Introduction

Non-Newtonian fluid flow in porous media has attracted a great attention for its applications in many engineering processes like oil recovery, petroleum extraction, industrial fluids, etc. In general, understanding non-Newtonian fluid flow is complex as compared to Newtonian fluids because of its complex rheology and shear stress may exhibit a different time dependent behavior. As a result, the numerical techniques have shifted their approach from the traditional continuum models to kinetic models. Continuum models focus on understanding flow properties in an elementary volume by considering fluid as a continuum, and thus, do not take into consideration individual particle behavior. Kinetic models, however, determine particle behavior and use averaging techniques so that the collective properties satisfy the macro-scale Navier-Stokes equations. A good research on non-Newtonian fluid flow in porous media is available in [1-6].

With the advances in computational technology, lattice Boltzmann method (LBM), a mesoscopic approach, has attracted a great attention to simulate complex flow processes like multiphase flows, non-Newtonian flow in porous media, etc. One of the advantages of LBM is its simple streaming and collision rules which decrease the number of mesh points by restricting the particle movement to only the lattice nodes. Implementation of boundary conditions, thus, is easier to impose at the meso-scale as compared to the macro-scale. Subsequently, LBM has been used extensively to a large number of problems in fluid dynamics [7-10].

Use of elevated temperatures to influence flow properties is well known in many applications such as groundwater flow and flow in porous media. Accordingly, many researchers have modified LBM to simulate forced convection in porous media. This is achieved by adding the effect of porous material to fluid flow by adding the total body force due to porous media and

the buoyancy effect as a result of temperature gradient. Appropriate methods are designed for velocity and thermal boundary conditions so that the boundary conditions are satisfied at the macro-scale. Peng et al. [11] proposed a simplified thermal LBM for incompressible thermal flow. Sullivan et al. [10, 12] validated use of LBM to simulate forced and natural convection in porous media using the LBM-BGK model. They used non-equilibrium rule of boundary conditions for the velocity and thermal distribution functions. Mehrizi et al. [13] presented effect of fin position and porosity on heat transfer in porous media. Shokouhmand et al. [14] simulated laminar flow and convective heat transfer between two parallel plates of a conduit using lattice Boltzmann method by employing a simplified thermal lattice BGK model with doubled population method. Gao et al. [15] proposed a thermal lattice Boltzmann model for natural convection in porous media under local thermal non-equilibrium conditions through an appropriate equilibrium distribution functions and discrete source terms. Research in this area is extensive and a large number of models have been proposed to simulate flow in porous media. However, no appropriate model has successfully described non-Newtonian fluid forced convection in porous media. This paper investigated forced convection in low permeable porous media (sandstones, sand) for non-Newtonian fluids. Practically, since the permeability of real geometries like sand, oil sands, etc. are very low, i.e., in the range of 10^{-10} to 10^{-6} [3], certain modifications in the numerical methods are necessary to achieve convergence. This will include identifying the parameters involved in the governing equations, applying suitable boundary conditions and varying relaxation parameter locally for convergence of the algorithm.

2. Governing Equations and Numerical Method

2.1. Governing equations

The generalized model for incompressible flow in porous media is given by Peng et al. [11]

$$\nabla \cdot u = 0, \tag{1a}$$

$$\frac{\partial u}{\partial t} + (u \cdot \nabla)\left(\frac{u}{\varepsilon}\right) = -\frac{1}{\rho}\nabla(\varepsilon p) + v_e \nabla^2 u + F, \tag{1b}$$

where ρ is the fluid density, u and p are the volume-averaged velocity and pressure, respectively. F is the total body force given by

$$F = -\frac{\varepsilon \nu}{K} u - \frac{\varepsilon F_\varepsilon}{\sqrt{K}} | u | u + \varepsilon(G), \tag{2}$$

where ν is the shear viscosity of the fluid and G is the body force. Permeability K and the Forchheimer's term F_ε are related to porosity ε (eps.) as described by Ergun [16]

$$F_\varepsilon = \frac{1.75}{\sqrt{150\varepsilon^3}}, \qquad K = \frac{\varepsilon^3 d_p^2}{150(1-\varepsilon)^2}, \tag{3}$$

where d_p is the solid particle diameter.

2.2. Lattice Boltzmann method

For incompressible fluid flows and a nine-velocity model on a two-dimensional lattice (D2Q9), the LBM model is given by Guo and Zhao [8]

$$f_i(x + e_i dt, t + dt) - f_i(x, t) = \frac{f_i^{eq}(x, t) - f_i(x, t)}{\tau} + dt F_i, \tag{4}$$

where dt is the time, τ is the relaxation time. $f_i^{eq}(x, t)$ is the equilibrium distribution function for D2Q9 given by

$$f_i^{eq}(x, t) = w_i \rho(x, t)\left[1 + \frac{1}{c_s^2}(e_i \cdot u(x, t)) + \frac{1}{2\varepsilon c_s^4}(e_i \cdot u(x, t))^2 - \frac{u(x, t)^2}{2\varepsilon c_s^2}\right]. \tag{5}$$

The force term F_i is given by [4]

$$F_i = w_i \rho\left(1 - \frac{1}{2\tau}\right)\left[\frac{e_i \cdot F}{c_s^2} + \frac{uF : (e_i e_i - c_s^2 I)}{\varepsilon c_s^2}\right]. \tag{6}$$

The fluid velocity u is given by

$$u = \frac{u_t}{c_0 + \sqrt{c_0^2 + c_1 | u_t |}}, \tag{7}$$

where u_t is a temporal velocity given by

$$u_t = \sum_i e_i f_i + \frac{dt}{2} \rho \varepsilon G. \tag{8}$$

The two parameters are given by

$$c_0 = \frac{1}{2}\left(1 + \varepsilon \frac{dt}{2} \frac{v}{K}\right), \quad c_1 = \varepsilon \frac{dt}{2} \frac{F_E}{\sqrt{K}}. \tag{9}$$

2.3. Energy equation

The thermal lattice BGK model proposed by Peng et al. [11] is used to model heat transfer

$$g_i(x + e_i dt, t + dt) - g_i(x, t) = \frac{g_i^{eq}(x, t) - g_i(x, t)}{\tau_g}, \tag{10}$$

$g_i(x, t)$ is the thermal distribution function, τ_g is the relaxation time and $g_i^{eq}(x, t)$ is the equilibrium distribution function given by [3, 11]

$$g_0^{eq}(x, t) = -\frac{2\rho\varepsilon}{3} \frac{u^2}{c_s^2}, \tag{11a}$$

$$g_i^{eq}(x, t) = \frac{\rho\varepsilon}{9}\left[\frac{3}{2} + \frac{3}{2}\frac{e_i \cdot u}{c_s^2} + \frac{9}{2}\frac{(e_i \cdot u)^2}{c_s^4} - \frac{3}{2}\frac{u^2}{c_s^2}\right] \quad (i = 1, 2, 3, 4), \tag{11b}$$

$$g_i^{eq}(x, t) = \frac{\rho\varepsilon}{36}\left[3 + \frac{6}{2}\frac{e_i \cdot u}{c_s^2} + \frac{9}{2}\frac{(e_i \cdot u)^2}{c_s^4} - \frac{3}{2}\frac{u^2}{c_s^2}\right] \quad (i = 5, 6, 7, 8), \tag{11c}$$

Reynolds number, $\mathrm{Re} = \frac{UL}{\upsilon}$, where U and L are the characteristic velocity and the characteristic length, respectively.

2.4. Boundary conditions

Second order bounce back rule for non-equilibrium distribution function f_i is used to determine velocity on the four walls. The distribution functions are given by Seta et al. [12]

$$f_{\alpha}^{neq} = f_{\beta}^{neq}, \tag{12}$$

where β is the opposite direction of α.

For energy distribution function g_i, second order extrapolation rule is used on the left wall and the boundary conditions for all other walls were defined as per method introduced by D'Orazio et al. [17]. The distribution functions on right wall were defined as

$$g_1 = \frac{6}{9}(1 - T_p), \quad g_5 = \frac{1}{36}T^{eq}(1 + 3(u + v)),$$

$$g_8 = \frac{1}{36}T^{eq}(1 + 3(u - v)), \tag{13a}$$

where $T_p = g_0 + g_2 + g_3 + g_4 + g_6 + g_7$ and

$$T^{eq} = \frac{6(1 - T_p)}{1 + 3u}. \tag{13b}$$

The distribution functions on the top wall were defined as

$$g_4 = \frac{1}{9}T^{eq}(1 + 3u), \quad g_7 = \frac{1}{36}T^{eq}(1 + 3(u + v)),$$

$$g_8 = \frac{1}{36}T^{eq}(1 + 3(u - v)), \tag{14a}$$

where $T_p = g_0 + g_1 + g_2 + g_3 + g_5 + g_6$ and

$$T^{eq} = \frac{-6T_p}{1 + 3u}. \tag{14b}$$

The distribution functions on the bottom wall were defined as

$$g_2 = \frac{1}{9}T^{eq}(1+3u), \quad g_5 = \frac{1}{36}T^{eq}(1+3(u+v)),$$

$$g_6 = \frac{1}{36}T^{eq}(1+3(u-v)), \tag{15a}$$

where $T_p = g_0 + g_1 + g_3 + g_4 + g_7 + g_9$ and

$$T^{eq} = \frac{-6T_p}{1+3u}. \tag{15b}$$

2.5. Problem description and numerical implementation

Fluid flows through a square geometry containing porous media with the left wall kept at a normalized temperature and all other walls adiabatic. Fluid enters the geometry with uniform velocity U through the left wall along horizontal direction. Permeability and porosity vary between 10^{-10} to 10^{-6} and 0.1 to 0.7, respectively, to match the geometrical properties of oil sands. Reynolds number Re and Prandtl number Pr are taken as 0.01 and 3.8 (of water), respectively. The relaxation parameter τ is initially set as 1.5. Carreau-Yasuda model is used to represent non-Newtonian fluids given by [18]

$$\mu = \mu_0 + (\mu_0 - \mu_\infty)/(1 + a(\dot{\gamma})^b)^{\frac{n-1}{b}}, \tag{16}$$

where μ_0 and μ_∞ are viscosities at zero and infinite shear rates, respectively. The parameters a and b along with μ_0 and μ_∞ should be appropriately defined for numerical simulation to converge which depends on index n and material properties of the porous media.

3. Results and Discussion

For non-Newtonian fluids, Darcy's law for fluid flowing through a porous media is given by [9]

$$q = \left(\frac{K}{\mu_{eff}} \frac{\nabla p}{L} \right)^{1/n}, \tag{17}$$

where q is Darcy flux, μ_{eff} is the effective viscosity. K and μ_{eff} depend on material properties of the porous media. ∇p is the pressure gradient and L is the characteristic length. Thus, validity of the numerical procedure for non-Newtonian numerical simulation can be established by verifying that the plot of q and $\nabla p = grad(p)$ is linear with slope $1/n$ as given in Table 1. The convergence of numerical simulation depends on how appropriately the parameters involved in equation (16) are selected. The relaxation parameter is varied locally, depending on the local strain, to identify the local flow properties at kinetic level so that the averaged flow parameters satisfy governing equations at macro level. The local definition of shear rate is given by [17]

$$\gamma_{\alpha\beta} = \frac{-3}{2\rho c^2 \tau dt} \sum_i e_{i\alpha} e_{i\beta} (f_i - f_i^{eq}). \tag{18}$$

Parameters μ_0 and μ_∞ determine the range of values for τ. Very low values of μ_0 may take τ close to 0.5 which makes the numerical method unstable. Similarly, high values of μ_∞ increase the value of τ reducing accuracy of the method. Thus, μ_0 and μ_∞ are set in the range of 0.001 and 0.1. Parameters a and b in equation (14) are varied in the ranges 10^{-7} to 10^{-4} and 0.67 to 10, respectively, depending on the values of n and K.

Table 1. Slope values for plot of q versus ∇p

n	K	ε		
		0.1	0.4	0.7
0.5	10^{-6}	1.9802	1.9889	1.9902
	10^{-8}	2.1092	2.0152	1.9921
	10^{-10}	1.9764	1.9794	1.9823
1	10^{-6}	1.0177	1.0133	1.0025
	10^{-8}	1.0177	1.0133	1.0025
	10^{-10}	1.0177	1.0133	1.0025
1.5	10^{-6}	0.7184	0.7169	0.7147
	10^{-8}	0.6442	0.6538	0.6602
	10^{-10}	0.6842	0.6813	0.6802

Figure 1 presents u-velocity profiles at the center of the cavity for shear-thinning fluids with $n = 0.5$ for various values of porosity ranging from 0.1 to 0.7 and permeability ranging from 10^{-10} to 10^{-6}. Influence of permeability and porosity can be observed on velocity as u-velocity decreases with decrease in permeability and increases with increase in porosity. This is in accordance with the rheological behavior of fluid flowing through porous media. Figures 2 and 3 present the variation in u-velocity as n is varied from 0.5 to 1.5. The u-velocity is observed to vary in proportion to the variation in permeability. In case of $n = 1$, the magnitude by which u-velocity decreases is equal to the magnitude by which permeability is varied. The magnitude of u-velocity increases with an increase in ε.

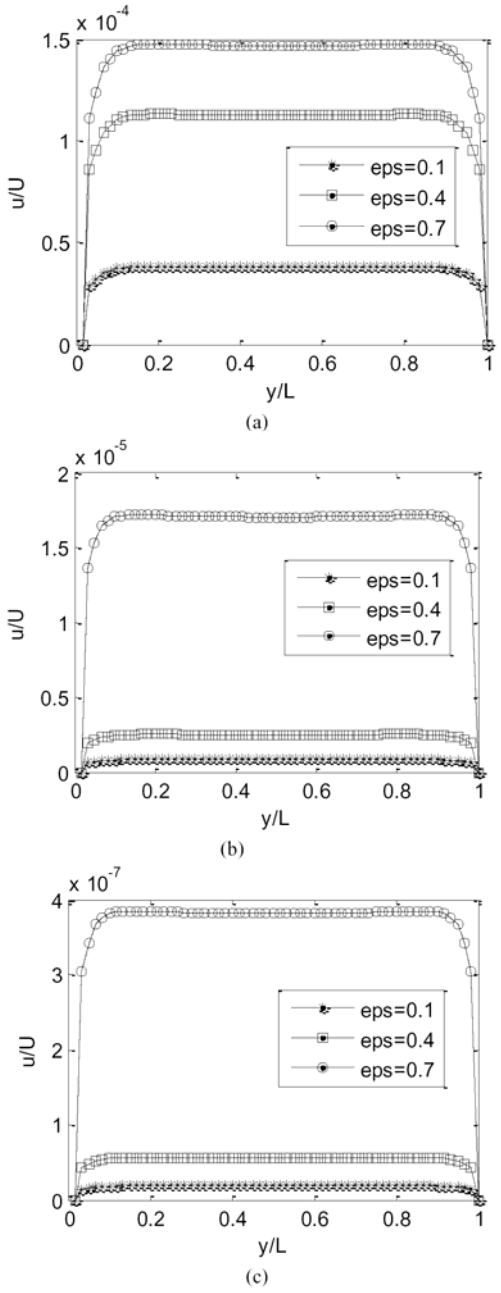

Figure 1. Normalized *u*-velocity profiles for different values of ε at $n = 0.5$ for (a) $K = 10^{-6}$, (b) $K = 10^{-8}$ and (c) $K = 10^{-10}$.

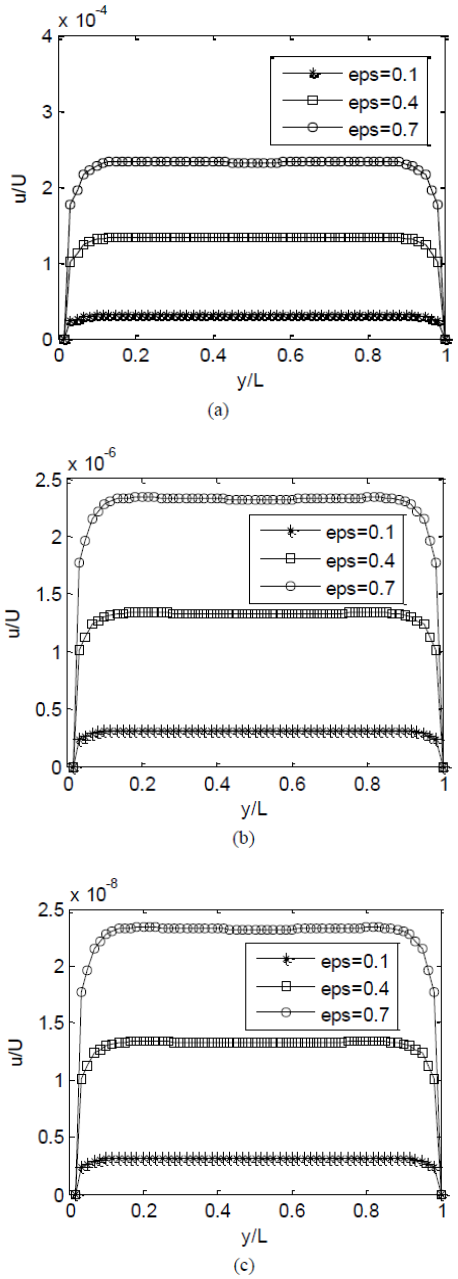

Figure 2. Normalized *u*-velocity profiles for different values of ε at $n = 1$ for (a) $K = 10^{-6}$, (b) $K = 10^{-8}$ and (c) $K = 10^{-10}$.

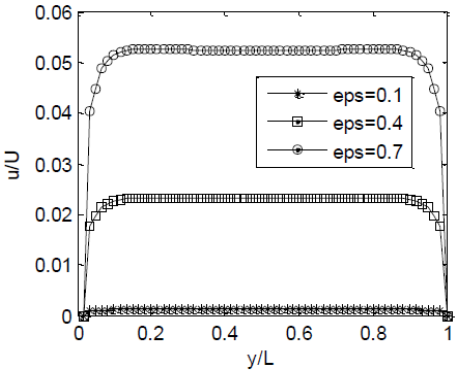

(a)

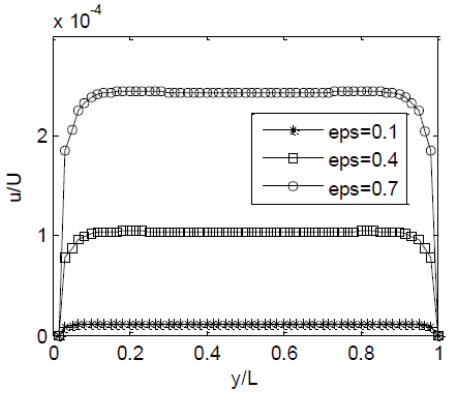

(b)

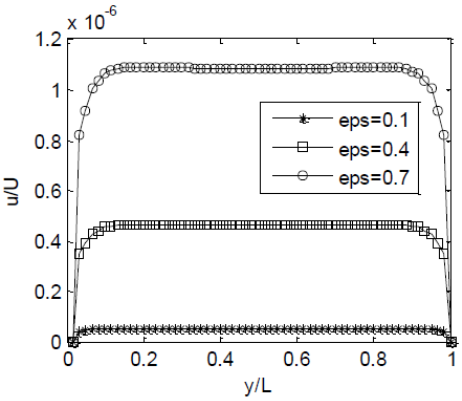

(c)

Figure 3. Normalized *u*-velocity profiles for different values of ε at $n = 1.5$ for (a) $K = 10^{-6}$, (b) $K = 10^{-8}$ and (c) $K = 10^{-10}$.

That is because of a bigger void proportion of porous media contributing in fluid flow. In reality, fluid flows in low permeable porous media at a very low velocity. Values of Nusselt number (Nu) at left wall are presented in Table 2. As observed, Nu tends to decrease as n increases from 0.5 to 1.5. As ε increases from 0.1 to 0.7, Nu also increases indicating a stronger heat transfer. Natural porous media are not found to have porosity more than 0.7, and thus, neglected for consideration. For shear-thinning fluid, apparent viscosity is inversely proportional to the strain, contributing to a more efficient convection process. As a result, the temperatures at the three axial positions for $n = 0.5$ are much higher as compared to $n = 1$ and $n = 1.5$ indicating a stronger heat transfer through fluid for shear-thinning fluids.

Table 2. Values of Nu at the hot wall

n	K	ε		
		0.1	0.4	0.7
0.5	10^{-6}	18.0768	19.0784	21.0792
	10^{-8}	18.0778	19.0841	21.0818
	10^{-10}	18.0818	19.7641	21.0965
1	10^{-6}	18.0756	18.0756	18.0756
	10^{-8}	18.0756	18.0756	18.0756
	10^{-10}	18.0756	18.0756	18.0756
1.5	10^{-6}	17.5633	17.7335	17.9803
	10^{-8}	17.5859	17.7589	17.9861
	10^{-10}	17.5961	17.7700	17.9970

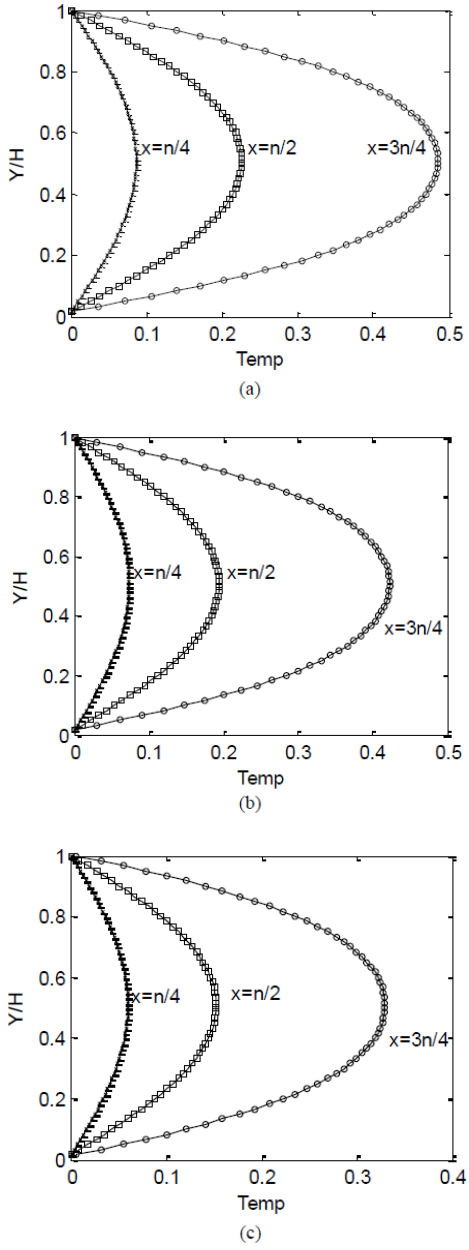

Figure 4. Variation in temperature profiles for different values of n for $\varepsilon = 0.1$, $K = 10^{-6}$ at three different axial positions for (a) $n = 0.5$, (b) $n = 1$ and (c) $n = 1.5$.

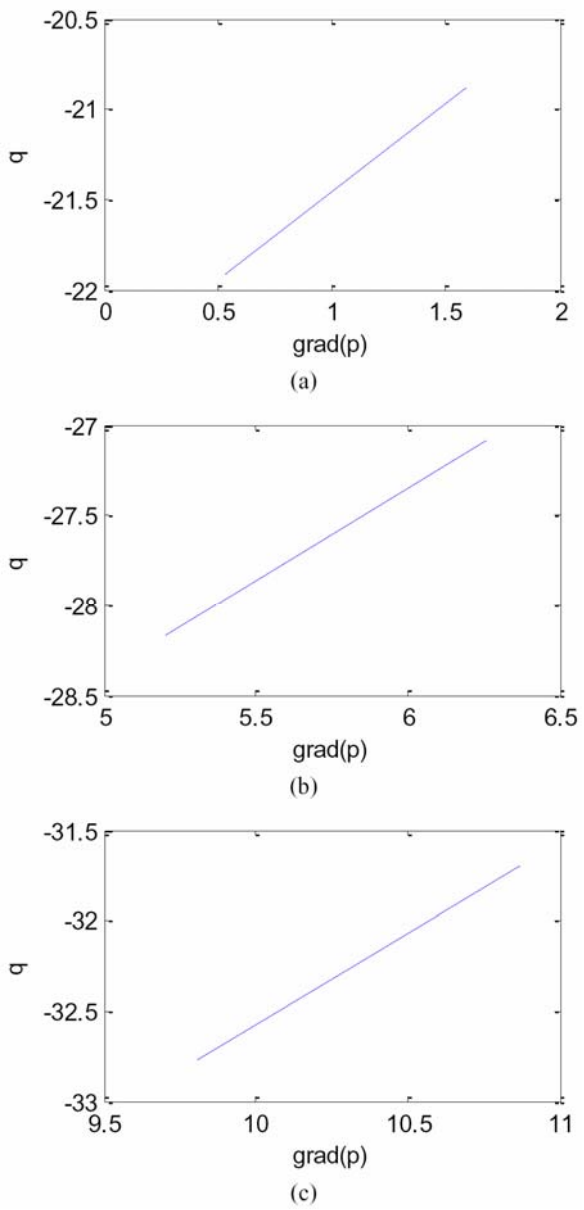

Figure 5. Plot of q versus ∇p for different values of K for $n = 1$ for (a) $K = 10^{-6}$, (b) $K = 10^{-8}$ and (c) $K = 10^{-10}$.

Figure 4 presents the variation in temperature at three different positions of the cavity with respect to power-law index n for $K = 10^{-6}$.

As the value of n increases from 0.5 to 1.5, the viscosity tends to increase resulting in a weaker convection of heat through fluid. These observations are also indicated by the variation of Nu with respect to n. Influence of permeability is also observed on flow properties, as indicated by the velocity profiles. However, its influence is not as significant as n, which is because of the fact that fluid in such geometries flows at a very low velocity. Figure 5 presents the plots of q versus ∇p. For the sake of space, only the plots for $n = 1$ are presented. Plots show a linear relationship with slope $1/n$. The relaxation parameter is used to determine the effective viscosity at micro-level, so that the averaged values satisfy the macro governing equations. Table 3 presents the average τ depending on the values of n, ε and K.

Table 3. Values of τ for various values of n, ε and K

n	K	ε		
		0.1	0.4	0.7
0.5	10^{-6}	1.7927	2.9790	3.6364
	10^{-8}	1.4909	2.1952	3.1189
	10^{-10}	1.4908	2.1327	3.0115
1	10^{-6}	1.4900	1.4900	1.4900
	10^{-8}	1.4900	1.4900	1.4900
	10^{-10}	1.4900	1.4900	1.4900
1.5	10^{-6}	1.4898	1.6396	1.4990
	10^{-8}	1.4639	1.0810	1.4668
	10^{-10}	1.4588	1.0807	1.4664

4. Conclusion

The paper investigated the influence of material properties of porous media on forced convection in non-Newtonian fluids. Permeability and porosity were varied in the range 10^{-10} to 10^{-6} and 0.1 to 0.7, respectively, to match the geometries of low permeable porous media like sandstones, sand, etc. Relaxation parameter is locally varied to achieve convergence of the numerical method and parameters involved in Carreau model are appropriately selected for stability of the algorithm. Velocity and temperature profiles are investigated to study the influence of permeability, porosity and the power-law index on flow properties. For shear-thickening fluids, heat transfer at low porosity is dominated by conduction while for higher values of porosity, it is dominated by convection.

References

[1] J. Bear, Dynamics of Fluids in Porous Media, Elsevier, New York, 1972.

[2] A. E. Scheidegger, The Physics of Flow through Porous Media, University of Toronto Press, Toronto, 1974.

[3] A. Bejan and D. A. Nield, Convection in Porous Media, Springer Science+Business Media, New York, 2013.

[4] J. G. Savins, Non-Newtonian flow through porous media, Industrial and Engineering Chemistry 61(2) (1969), 18-47.

[5] J. R. A. Pearon and P. M. J. Tardy, Models for flow of non-Newtonian and complex fluids through porous media, J. Non-Newtonian Fluid Mech. 102 (2002), 447-473.

[6] Sochi Taha, Non-Newtonian flow in porous media, Polymer 51 (2020), 5007-5023.

[7] Shiyi Chen and G. D. Doolen, Lattice Boltzmann method for fluid flows, Ann. Rev. Fluid Mech. 30(1) (1998), 329-364.

[8] Zhaoli Guo and T. S. Zhao, Lattice Boltzmann model for incompressible flows through porous media, Phys. Rev. E 66 (2002), 036304.

[9] T. Seta, E. Takegoshi and K. Okui, Lattice Boltzmann simulation of natural convection in porous media, Math. Comput. Simulation 72 (2006), 195-200.

[10] S. P. Sullivan, L. F. Gladden and M. L. Johns, Simulation of power-law flow through porous media using lattice Boltzmann techniques, J. Non-Newtonian Fluid Mech. 133 (2006), 91-98.

[11] Y. Peng, C. Shu and Y. T. Chew, Simplified thermal lattice Boltzmann model for incompressible thermal flow, Phys. Rev. E 68 (2003), 046308.

[12] T. Seta, E. Takegoshi, K. Kitano and K. Okui, Thermal lattice Boltzmann model for incompressible flows through porous media, Journal of Thermal Science and Technology 1(2) (2006), 90-100.

[13] A. Abouei Mehrizi, M. Farhadi, K. Sedighi and M. Aghajani Delavar, Effect of fin position and porosity on heat transfer improvement in a plate porous media heat exchanger, Journal of the Taiwan Institute of Chemical Engineers 44 (2013), 420-431.

[14] H. Shokouhmand, F. Jam and M. R. Salimpour, Simulation of laminar flow and convective heat transfer in conduits filled with porous media using lattice Boltzmann method, International Communications in Heat and Mass Transfer 36 (2009), 378-384.

[15] Dongyan Gao, Zhenqian Chen and Linghai Chen, A thermal lattice Boltzmann model for natural convection in porous media under local thermal non-equilibrium conditions, International Journal of Heat and Mass Transfer 70 (2014), 979-989.

[16] S. Ergun, Flow through packed columns, Chemical Engineering Process 48 (1952), 89-94.

[17] A. D'Orazio, M. Corcione and G. P. Celata, Application to natural convection enclosed flows of a lattice Boltzmann BGK model coupled with a general purpose thermal boundary condition, Int. J. Therm. Sci. 43(6) (2004), 575-586.

[18] C. R. Leonardi, D. R. J. Owen and Y. T. Feng, Numerical rheometry of bulk materials using a power-law fluid and the lattice Boltzmann method, J. Non-Newtonian Fluid Mech. 166 (2011), 628-638.